The Pore Domain of the Nicotinic Acetylcholine Receptor: Molecular Modeling, Pore Dimensions, and Electrostatics

R. Sankararamakrishnan, C. Adcock, and Mark S. P. Sansom
Laboratory of Molecular Biophysics, University of Oxford, Oxford OX1 3QU, UK

ABSTRACT The pore domain of the nicotinic acetylcholine receptor has been modeled as a bundle of five kinked M2 helices. Models were generated via molecular dynamics simulations incorporating restraints derived from 9-Å resolution cryoelectron microscopy data (Unwin, 1993; 1995), and from mutagenesis data that identify channel-lining side chains. Thus, these models conform to current experimental data but will require revision as higher resolution data become available. Models of the open and closed states of a homopentameric $\alpha 7$ pore are compared. The minimum radius of the closed-state model is less than 2 Å; the minimum radius of the open-state model is ~6 Å. It is suggested that the presence of "bound" water molecules within the pore may reduce the effective minimum radii below these values by up to ~3 Å. Poisson-Boltzmann calculations are used to obtain a first approximation to the potential energy of a monovalent cation as it moves along the pore axis. The differences in electrostatic potential energy profiles between the open-state models of $\alpha 7$ and of a mutant of $\alpha 7$ are consistent with the experimentally observed change in ion selectivity from cationic to anionic. Models of the open state of the heteropentameric *Torpedo* nicotinic acetylcholine receptor pore domain are also described. Relatively small differences in pore radius and electrostatic potential energy profiles are seen when the *Torpedo* and $\alpha 7$ models are compared.

INTRODUCTION

The nicotinic acetylcholine receptor (nAChR) mediates signal transmission at chemical synapses (Stroud et al., 1990; Changeux et al., 1992; Lester, 1992; Galzi and Changeux, 1994; Montal, 1995) and is the best characterized member of the superfamily of neurotransmitter-gated ion channels. The intact nAChR has five subunits, surrounding a cation-selective, water-filled pore. In muscle nAChR the channel-forming assembly is heteropentameric (subunit stoichiometry $\alpha_2\beta\gamma\delta$), whereas neuronal nAChR appears to have simpler stoichiometries. In particular, the $\alpha 7$ neuronal nAChR may form homopentameric (α_5) assemblies, at least in vitro (Couturier et al., 1990; Sivilotti and Colquhoun, 1995). Each nAChR subunit contains four hydrophobic segments (M1 to M4). Photolabeling experiments using open channel blockers (Hucho et al., 1986; Giraudat et al., 1987) and site-directed mutagenesis studies (Imoto et al., 1988; Leonard et al., 1988; Charnet et al., 1990; Villarroel et al., 1991) suggest that the second segment (M2) is a transmembrane helix that forms part of the lining of the channel. Synthetic peptides corresponding to the M2 sequence form transbilayer α-helices that self-assemble in lipid bilayers to form cation channels whose properties resemble those of the parent channel protein (Oiki et al., 1988). Together, these studies suggest that the nAChR pore is lined by a bundle of five M2 helices.

Electron microscopic studies of the closed (Unwin, 1993, 1996) and open (Unwin, 1995) states of *Torpedo* nAChR at 9-Å resolution reveal that five rods of density, one from each subunit, form an approximately parallel bundle surrounding a central pore (Sansom et al., 1995a). These rods have been identified with the bundle of five M2 helices. In the open state of nAChR, the pore is formed by a right-handed supercoil of α-helices. In the closed state, the M2 helices twist around each other in a left-handed fashion. In both conformations of the receptor the M2 helices are not straight, but are kinked in the vicinity of their central leucine (L11′; for the numbering scheme of residues see Fig. 1 and below) residue. It has been suggested that in the closed channel the L11′ side chains form a hydrophobic ring that presents a barrier to the permeation of cations (Unwin, 1993), although alternative gating mechanisms are possible (Karlin and Akabas, 1995).

In a previous paper (Sansom et al., 1995a) restraints derived from the 9-Å resolution structure of the closed nAChR were used to generate an atomic-level model of the M2 helix bundle of a neuronal ($\alpha 7$) receptor in its closed state. Models were generated using simulated annealing via restrained molecular dynamics (SA/MD). In the current study we extend this approach to the M2$\alpha 7$ helix bundle in its open state and compare the resultant open- and closed-state models. We also model the open state of a mutant of $\alpha 7$ that has been shown to have altered ion selectivity (Galzi et al., 1992), and describe models for the open state of the *Torpedo* nAChR. The models are analyzed in terms of their pore dimensions and electrostatic profiles. Of course, it must be remembered that the available data do not yield a large enough body of restraints to fully define the geometry of the pore. Thus, although these models conform to current

Received for publication 22 April 1996 and in final form 10 July 1996.

Address reprint requests to Dr. M. S. P. Sansom, Laboratory of Molecular Biophysics, The Rex Richards Building, University of Oxford, South Parks Road, Oxford OX1 3QU, England. Tel.: +44-1-865-275371; Fax: +44-1-865-510454; E-mail: mark@biop.ox.ac.uk.

Dr. Sankararamakrishnan's current address is Department of Physiology and Biophysics, Beckman Institute, University of Illinois at Urbana-Champaign, Urbana, IL 61801.

0006-3495/96/10/1659/13 $2.00

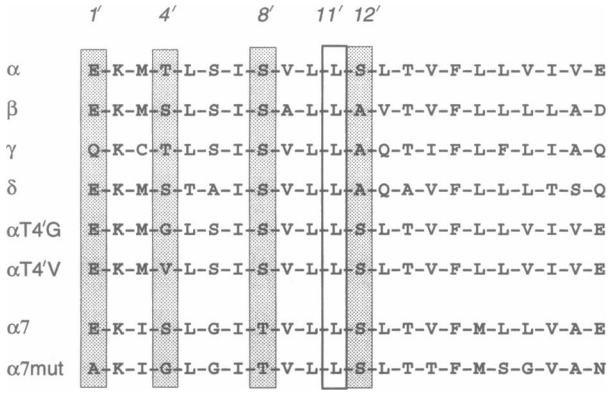

FIGURE 1 Sequences of the M2 helices used in models of the nAChR pore domain. α, β, γ, and δ are the M2 sequences of the four *Torpedo* subunits; $\alpha 7$ is the sequence of M2 of the chick $\alpha 7$ nAChR; and $\alpha 7$ *mut* is the sequence of M2 for an anion selective mutant of chick $\alpha 7$ nAChR (Galzi et al., 1992). Key residues lining the pore in the open conformation of the channel are enclosed in the stippled box; the conserved leucine implicated in closing the channel is indicated by the white box.

experimental data, they almost certainly will require revision as higher resolution data become available.

METHODS

Programs

Molecular dynamics (MD) simulations and model building were carried out using Xplor V3.1 (Brünger, 1992) with the CHARMm PARAM19 (Brooks et al., 1983) parameter set. Only those H atoms attached to polar groups were represented explicitly; apolar groups were represented using extended carbon atoms. Display and examination of models were carried out using Quanta V4.1 (Molecular Simulations), and diagrams of structures were drawn using Molscript (Kraulis, 1991). Pore dimensions were calculated using HOLE (Smart et al., 1993), and electrostatics calculations employed UHBD version 5.1 (Davis et al., 1991). MD simulations were performed on a DEC 3000 400 computer. All other calculations were carried out on Silicon Graphics workstations.

Simulated annealing via restrained molecular dynamics

Our implementation of simulated annealing via restrained molecular dynamics (SA/MD) has already been described in detail (Kerr and Sansom, 1993; Kerr et al., 1994; Breed et al., 1995; Sankararamakrishnan and Sansom, 1995ab; Sansom and Kerr, 1995; Sansom et al., 1995a,b), and so only a brief account is provided here. Furthermore, as the modeling of the closed state of the nAChR pore has already been described (Sansom et al., 1995a), the following description applies specifically to modeling the open state.

SA/MD was carried out in two stages. In Stage 1 a slow annealing protocol was used to generate approximate coordinates for the polypeptide backbone and side chains, while the overall Cα coordinates of the helices remained fixed. The starting point for Stage 1 of SA/MD was a Cα template corresponding to an exactly parallel bundle of five ideal α-helices, in which the backbone and side-chain atoms were superimposed upon the Cα atoms of the corresponding residues. Stage 2 was a restrained MD simulation, during which the helices were allowed to move and backbone and side-chain conformations were refined. Five structures from Stage 1 were each subjected to five restrained MD runs during Stage 2, resulting in a final ensemble of $5 \times 5 = 25$ structures. Target and distance restraints were imposed during Stage 2 to optimize the fit of the models to experimental structural and mutagenesis data.

Restraints

Three possible classes of restraint were used during Stage 2 of SA/MD: 1) intrahelix distance restraints; 2) interhelix distance restraints; and 3) structure-derived target restraints. Such restraints were imposed to 1) maintain an α-helical pattern of H-bonding within M2; 2) orient the 4′, 8′, and 12′ side chains toward the center of the bundle (see below); and 3) distort the helices toward the geometry seen in the electron microscopy (EM)-derived structure (Unwin, 1995), respectively.

Target restraints were used to distort the M2 helices toward the kinked geometry observed in the 9-Å open-state structure (Unwin, 1995). Target restraints were implemented in the same manner as in our previous study of the closed state (Sansom et al., 1995a), by using a harmonic potential energy function:

$$E_{\mathrm{HARM}} = H \sum_{\mathrm{i}} (r_{\mathrm{i}} - r_{\mathrm{i}}^{\mathrm{REF}})^2,$$

in which r_{i} is the coordinate of Cα atom i, $r_{\mathrm{i}}^{\mathrm{REF}}$ is the corresponding coordinate in the target structure, and where $H = 4.0$ kcal mol^{-1}Å^{-2} is the force constant determining the strength of the restraints necessary to achieve a good fit to the target coordinates. Restraints were implemented by setting up target Cα coordinates corresponding to the helix positions in the EM structure. Summation in the above equation is across all Cα coordinates of the helix bundle.

The target Cα coordinates were derived from density sections of the EM-derived structure (kindly provided by Dr. N. Unwin). Display of these coordinates on a graphics terminal revealed that the density for each kinked M2 helix could be approximated as two straight line segments intersecting at the presumed position of L11′. Equations for the two line segments were used to obtain target Cα coordinates in the same manner as in the method of Sansom et al. (1995a). Note that the target Cα coordinates for each kinked M2 helix thus lie on one of the two straight line segments. When harmonic restraints are applied using such a target and the chosen value of H, the Cα atoms of each M2 helix segment in the resultant structure arrange themselves such that they lie approximately on the surface of a cylinder around the target coordinates, thus minimizing the value of E_{HARM}.

Electrostatics

The electrostatic potential around the M2 helix bundles was calculated via numerical solution of the Poisson-Boltzmann equation, using the program UHBD (Davis et al., 1991). The protein dielectric was set to 2 and the water dielectric to 78. The M2 helix bundle was set in a low-dielectric (2) slab to mimic the effect of the surrounding protein and lipid bilayer. The ionic strength was set to 100 mM. A 1-Å grid and a 2-Å Stern radius (Gilson et al., 1988) were used. The partial atomic charges and radii used in these calculations were the same as in the MD simulations, i.e., the standard Charmm values. All glutamate side chains were assumed to be in their $-1e$ charge state, and all lysine residues in their $+1e$ charge state. Electrostatic energy profiles were obtained by calculating the energy of a $+1e$ probe charge at successive positions along the center of the pore, as defined by HOLE calculations of the pore radius profile.

RESULTS

Modeling the $\alpha 7$ open state

For comparison with the closed-state model, the open state of a neuronal $\alpha 7$ nAChR pore was modeled. The homopentameric nature of this channel (Couturier et al., 1990) sim-

plifies the generation of a model for the pore. Furthermore, this channel has been the subject of extensive mutagenesis studies (Changeux et al., 1992; Galzi et al., 1992; Bertrand et al., 1993). The sequence of the M2α7 helix is given in Fig. 1. Note that throughout this paper the glutamate residue of the cytoplasmic *intermediate ring* (Imoto et al., 1988; Bertrand et al., 1993) is numbered as 1′. Thus, the leucine residue suggested to occlude the pore when the channel is in a closed conformation is L11′, and the hydroxyl-containing residues implicated in lining the pore of the open channel are residues 4′, 8′, and 12′. In all of our models the N-termini of the M2 helices are blocked with an acetyl group and the C-terminus with an amide group to mimic the effects of the preceding and following peptide bonds within the intact protein. The length of M2 and its position within the α7 nAChR sequence are consistent with current structural and mutagenesis data (Bertrand et al., 1993; Unwin, 1993).

In any modeling study it is important to state clearly the assumptions that are implicit within a model and are the experimental basis of these assumptions. Our first assumption is that residues 1′ to 22′ of M2 adopt an α-helical conformation. This is based primarily upon the EM data (Unwin, 1995), which are consistent with a pore lined by a bundle of five α-helices of length ~30 Å. The identification of these α-helices with M2 is supported by a wide range of chemical labeling (Hucho et al., 1986; Giraudat et al., 1987) and mutagenesis (Imoto et al., 1988; Leonard et al., 1988; Charnet et al., 1990; Villarroel et al., 1991; Cohen et al., 1992) data. Furthermore, Montal and colleagues have synthesized a 23-mer peptide corresponding to *Torpedo* M2δ (Oiki et al., 1988), and solid state NMR evidence (Bechinger et al., 1991) suggests that this peptide forms a transbilayer α-helix in lipid bilayers. The second assumption is that the M2 helices are oriented such that their N-termini correspond to the cytoplasmic face of the membrane. This is supported by, e.g., the mutagenesis data of Imoto et al. (1988), who measured the altered sensitivity to internal versus external Mg^{2+} of channels with mutations (to lysine) of the anionic side chains at the N-terminus versus the C-terminus of M2. The third assumption concerns the orientation of the side chains in the N-terminal segment of M2. Several mutagenesis studies (e.g., Leonard et al., 1988; Charnet et al., 1990; Villarroel et al., 1991; Cohen et al., 1992) have indicated that residues 4′, 8′, and 12′ (e.g., Leonard et al., 1988; Charnet et al., 1990; Villarroel et al., 1991) interact with permeant ions and/or open channel blockers. Thus it is reasonable to suppose that the N-terminal segments of M2 are oriented such that these side chains are directed toward the lumen of the pore when the latter is in its open state.

These assumptions are embodied in the restraints used in SA/MD. Thus, intrahelical distance restraints maintain M2 in an α-helical conformation. The N-to-C cytoplasmic-to-synaptic orientation of the helices is determined by the Cα template. The overall conformation and positions of the M2 helices are governed by the target restraints derived from the EM data. Last, the orientation within the N-terminal segments of residues 4′, 8′, and 12′ was maintained by placing appropriate interhelix distance restraints between the Cβ atoms of these side chains lying on opposite sides of the M2 helix bundle.

The resultant model of the open-state M2α7 bundle is shown in Fig. 2. Cα traces for five structures from the ensemble are shown superimposed upon the corresponding target restraints. Although there is evidently some variation between members of the ensemble (as reflected in a backbone atom RMSD of ~0.5 Å; Table 1), the agreement between the Cα traces and the target restraints is good. Thus it is possible to obtain a satisfactory fit of a bundle of α-helices to the EM-derived target restraints by SA/MD. Indeed, the value of E_{HARM} for the open-state model is somewhat lower than that for the previously described closed-state model of α7 (Table 1; Sansom et al., 1995a). The helices in the open-state α7 model have a central kink. The N-terminal helical segments form a right-handed supercoil, whereas the C-terminal segments do not form an appreciable supercoil but rather extend radially from the central axis. Thus, the overall structure of the M2 helix bundle is in good agreement with the EM structure, as is confirmed by overlaying the models with the 9-Å resolution density (not shown).

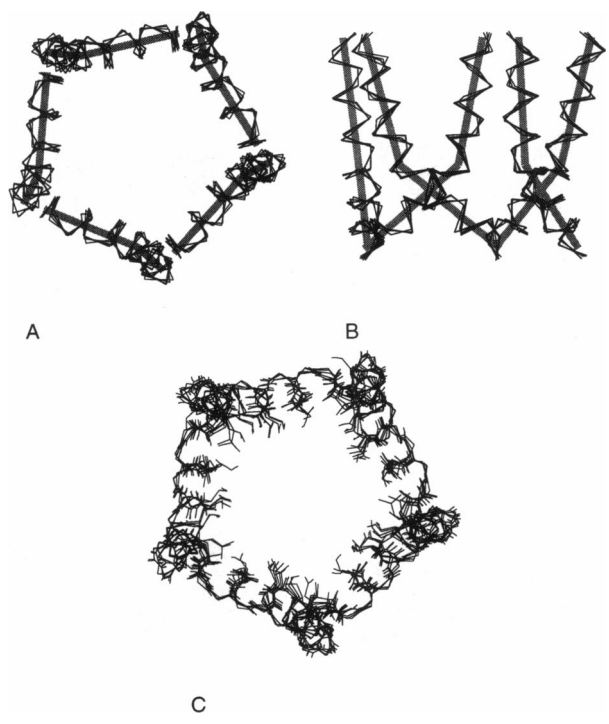

FIGURE 2 Comparison of the target restraints (*thick grey line*) and Cα traces for five superimposed structures (from an ensemble of 25) for the α7 open conformation model. The restraints were derived from the density of Unwin (1995), and the models were obtained by SA/MD (see text for details). (*A*) View down the pore (*z*) axis; (*B*) view perpendicular to the pore axis, with the C-termini of the helices uppermost. (*C*) All backbone atoms, plus the side chains at positions 1′, 4′, 8′, 11′, and 12′, are shown to illustrate the intra-ensemble variations in conformation.

TABLE 1 α7 closed and open models

Property	α7 closed model	α7 open model
Geometry		
RMSD (Å)	0.50	0.47
ϕ (°)	−66 (±11)	−66 (±6)
ψ (°)	−33 (±15)	−35 (±9)
ω (°)	+178 (±4)	+176 (±2)
D_{MIN} (Å)	12.6 (±0.4)	14.2 (±0.1)
θ_{KINK} (°)	46 (±2)	36 (±1)
Energetics		
E_{TOT} (kcal/mol)	−2232 (±61)	−2723 (±65)
E_{VDW} (kcal/mol)	−329 (±7)	−395 (±9)
E_{ELEC} (kcal/mol)	−2851 (±55)	−3071 (±65)
E_{HARM} (kcal/mol)	+722 (±8)	+564 (±1)
ΔE_{TOT} (kcal/mol)	−14 (±2)	−51 (±11)
ΔE_{VDW} (kcal/mol)	−14 (±2)	−45 (±6)
ΔE_{ELEC} (kcal/mol)	+1 (±0.3)	−7 (±6)
ΔA (Å^2)	−834 (±56)	−2170 (±70)

α7: comparison of open- and closed-state models

Selected structures from the closed- and open-state ensembles for the α7 models are shown in Fig. 3. It should be remembered that within a given ensemble there is variation in the conformations of the side chains, whereas in this diagram only single structures from each ensemble are shown. The first feature to note is the difference in the M2 helix backbone orientations between the open and closed states. In the closed-state model the apex of the kink of M2 is directed toward the pore and corresponds to a distortion of the α-helical backbone (see below). In the open state the apex of the kink is less distorted and is directed toward the helix-helix interface. This movement of the N-terminal segment of the M2 helix changes the positioning of the S4′, T8′, L11′, and S12′ side chains between the closed- and open-state models. In the closed state the L11′ side chains are directed toward the center of the pore, whereas the S4′, T8′, and S12′ side chains lie at the interfaces between adjacent helices. In the open-state model, the L11′ side chains are shifted to an interfacial location, whereas the S4′, T8′, and S12′ side chains form the lining of the N-terminal half of the pore. Thus, the open-state model is consistent with the mutagenesis-derived restraints and provides a pore with a highly polar lining to its narrowest region.

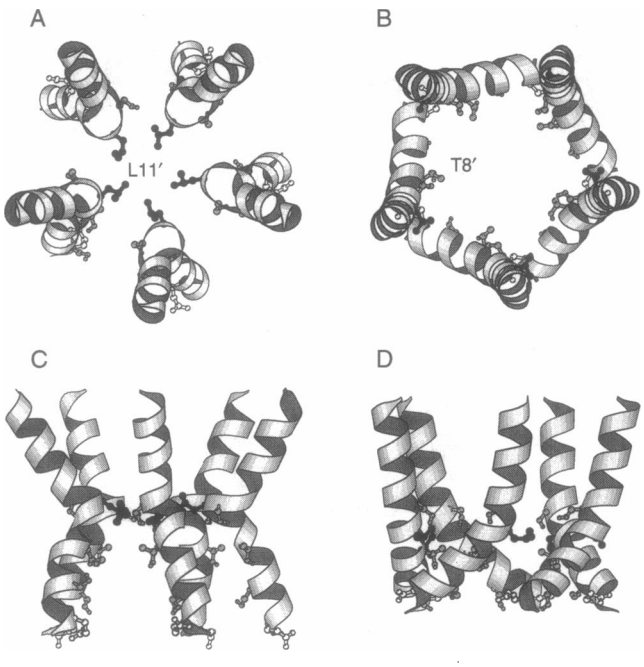

FIGURE 3 Ribbon diagrams of models of the α7 pore in the closed (*A* and *C*) and open (*B* and *D*) conformations. (*A* and *B*) View down the pore (*z*) axis, looking from the C-termini (extracellular) toward the N-termini (intracellular). (*C* and *D*) View perpendicular to the pore axis with the C-termini of the helices uppermost. Selected side chains are shown in "ball-and-stick" format: E1′ (*white*), S4′, T8′, S12′ (*grey*), and L11′ (*black*). This figure was generated using Molscript (Kraulis, 1991).

It is informative to compare the backbone conformations of the M2 helices in the open and closed models. Comparison of the Ramachandran plots (not shown) shows that in both models the torsion angles lie within the α-helical region, but suggest that the distortion of the α-helices is greater in the closed- than in the open-state model. In combination with visual examination of the two models, this suggests that the shift between the closed and open states does not simply correspond to a rigid body movement of the M2 helices, but rather that the region around L11′ may act as a "molecular swivel" (Sansom, 1995; Unwin, 1995). This is confirmed by a residue-by-residue analysis of the backbone torsion angles of the two models (Fig. 4), which demonstrates that for both the open and closed models the N- and C-terminal segments of M2 have α-helical conformations (also see Table 1). However, in the central region of the helices, around residue L11′, local distortion of the α-helical geometry occurs. This is more marked for the closed-state than for the open-state model. Furthermore, the pattern of distortions differs between the two models. This supports the notion of this region of M2 acting as a molecular swivel.

It is also instructive to examine the packing and energetics of the helices in the closed and open models (Table 1). The kink angles of the helices are similar in the two models. The axes of adjacent helices approach more closely in the closed state than in the open state. The large helix-helix interaxial separation (D_{MIN}) indicates the relatively loose packing of the helices. This is also seen in the weak energies of interaction between the constituent helices of a bundle (ΔE) and the small buried surface area. Helix-helix interactions are somewhat stronger for the open state, particularly in the N-terminal half of the pore, within which the M2 helices pack together rather more closely. Residue-by-residue analysis of buried surface areas indicates that the main residues buried at the helix-helix interface in the open-state model are E1′, L5′, I7′, and L11′. Thus in the open-state model the helix-helix interactions are mainly nonpolar in nature. The relatively loose packing of the C-terminal seg-

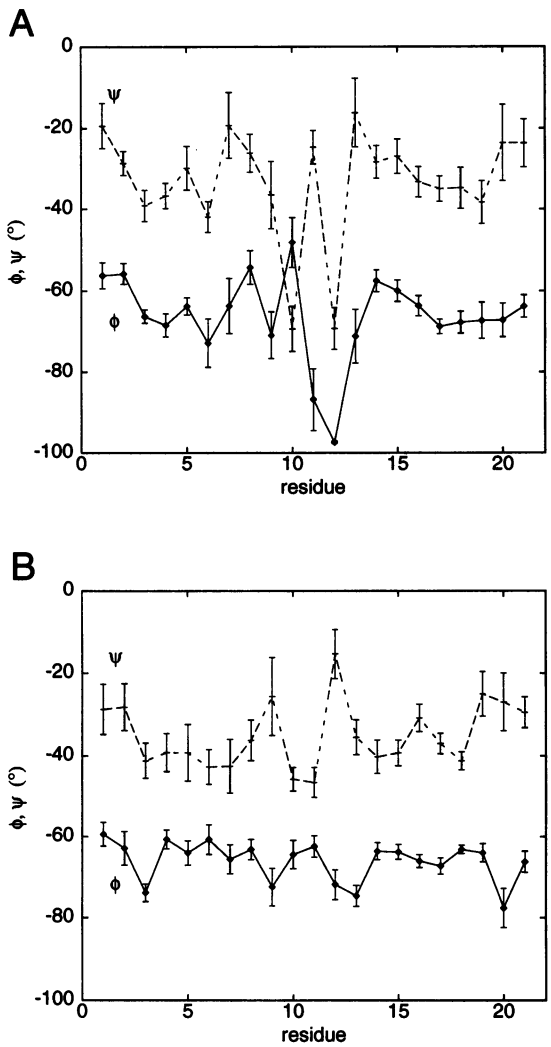

FIGURE 4 Backbone torsion angles versus residue number. Ensemble averages (±SD) of (ϕ,ψ) angles are shown for models of the α7 pore in the closed (*A*) and open (*B*) conformations.

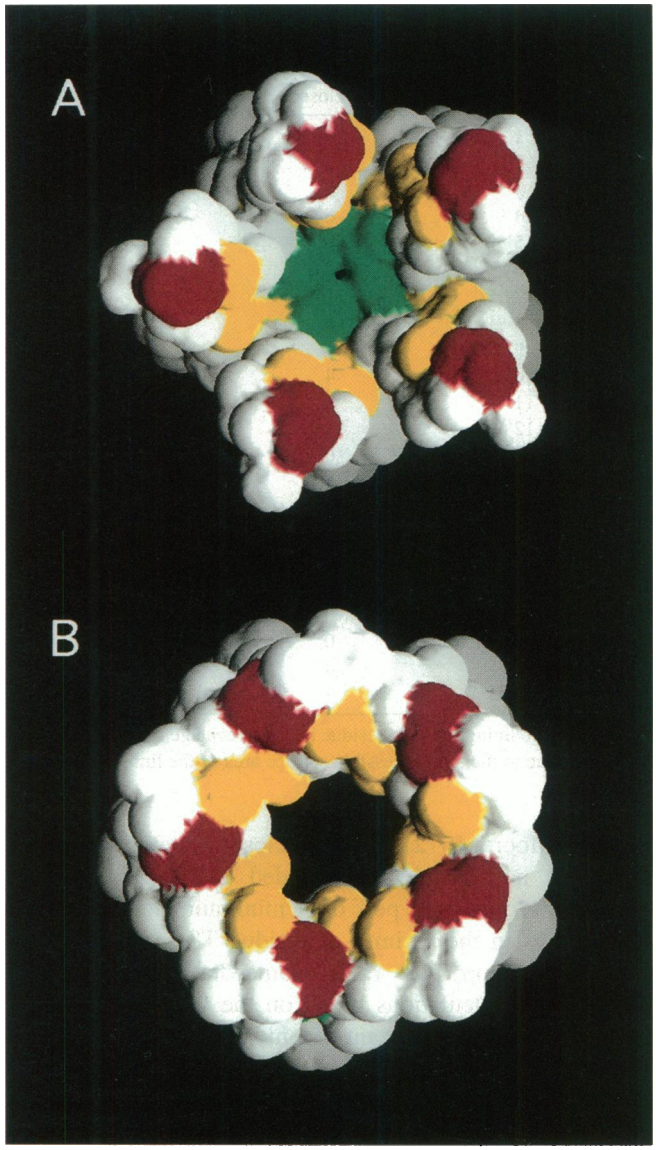

FIGURE 5 Solvent-accessible surfaces for the α7 model pore in the closed (*A*) and open (*B*) conformations. Pore lining residues are color coded: red = E1′; yellow = S4′, T8′, and S12′; green = L11′. This figure was generated using GRASP (Nicholls and Honig, 1992).

ments of the M2 helices may reflect the presence of the M1 segments within the intact protein (see Discussion).

Pore properties

The solvent-accessible surfaces of the α7 closed- and open-state pore models are compared in Fig. 5, in which the pore is viewed from the N-termini of the M2 helices looking outward. The relative contributions of the M2 side chains to the pore lining in the two conformations are summarized in Table 2. The difference in the dimensions and polarity of the pore is evident. Thus, in the closed state the lining of the N-terminal half of the pore is somewhat less polar, and the pore is occluded by the ring of L11′ side chains. In the open-state model, the pore is lined by the hydroxyl side chains of residues S4′, T8′, and S12′, and the L11′ side chains do not contribute appreciably to the pore lining. Furthermore, in the open-state model the swiveling of the N-terminal segments of the M2 helix brings the E1′ side chains more directly into the lining of the pore. We will now examine how these changes are reflected in the pore radius and electrostatic profiles.

Pore radius profiles for the closed- and open-state α7 models were calculated using HOLE (Smart et al., 1993). This translates to a sphere along the length of the pore (i.e., the *z*-axis), such that for each value of *z* the radius and *xy* coordinate of the center of the sphere are optimized to obtain the largest possible sphere in van der Waals contact with the pore. Radius profiles for the closed and open models are compared in Fig. 6 *A*. The minimum radius of the closed-state pore is less than 2 Å and occurs in the vicinity of residue L11′. Remember that the radius of a water molecule is ~1.4 Å and that of a hydrated Na^+ ion is

TABLE 2 Channel-lining residues

Residue	Percentage lining	
	α7, closed	α7, open
1′	10	9
2′	2	0
3′	5	2
4′	6	7
5′	6	4
6′	0	0
7′	7	3
8′	5	6
9′	1	4
10′	4	0
11′	8	0
12′	1	3
13′	0	3
14′	5	0
15′	7	5
16′	3	11
17′	2	0
18′	12	5
19′	6	12
20′	0	7
21′	4	0
22′	7	18

The percentage lining for each residue is the percentage contribution made by that residue to the total accessible surface area of the lining of the pore.

~2.4 Å (Moore, 1972). Thus the closed-state pore is effectively but not completely occluded (see Discussion). In contrast, the open-state pore has a minimum radius of ~6 Å. This occurs in the vicinity of residue T8′. Note that this gives a minimum pore radius somewhat larger than that indicated by calculations based on the van der Waals dimensions of large permeant organic cations (Dwyer et al., 1980; Nutter and Adams, 1995). This is discussed in more detail below (see Discussion). What is most striking from this comparison is that the minimum pore radius increases by more than 4 Å on going from the closed- to the open-state model, and the narrowest region of the pore shifts from the center of M2 (in the closed state) toward the N-terminal segment (in the open state). Note also that variations in side-chain conformations between the different members of each ensemble do not give rise to very large variations in the pore radius profiles (as indicated by the error bars in Fig. 6).

To evaluate the success of the α7 open-state pore model in explaining experimental observations, we have also modeled a mutant nAChR pore domain. We have chosen to model the M2 helix bundle (Fig. 1) of an α7 mutant shown by Galzi et al. (1992) to alter the ion selectivity of the channel from cationic to anionic. Note that this mutant has the sequence of M2α7 changed at several positions: E1′A, S4′G, V15′T, and E22′N. Thus the main change is that of neutralization of negative charges at either mouth of the pore, but there are also additional changes within the center of the M2 helix. An ensemble of *α7 mut* open-state structures was generated by running SA/MD in the same way as for the α7 open state, but substituting the sequence of the mutant for that of the wild-type channel. Thus, this simulation was based on the assumption that the mutant sequence did not result in a global conformational change in M2. Interhelix distance restraints were only applied to the Cβ-Cβ distances of residues 8′ and 12′ during the *α7 mut* simulation (because of the glycine at position 4′). The pore radius profiles for the open state of α7 and of *α7 mut* are compared in Fig. 6 *B*. Small but significant changes in the radius profile can be seen. The minimum radius is not greatly altered, but in *α7 mut* the constriction has moved slightly toward the N-terminus. The pore is somewhat narrower for *α7 mut* at $z \approx 16$ Å, i.e., in the vicinity of the V15′T change. In both models there is significant intra-ensemble variation in the pore radius in this region, reflecting possible alternative conformations for the F16′ side chain. The *α7 mut* pore is also a little wider at the C-terminal mouth.

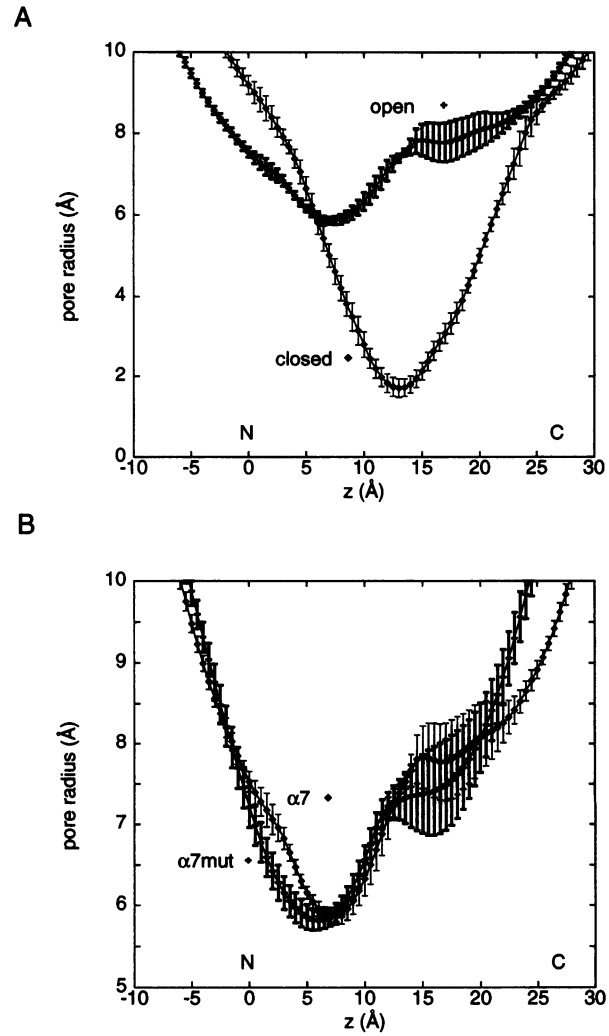

FIGURE 6 Pore radius profiles. (*Top*) The pore radius as a function of distance along the pore (z) axis is compared for the closed (◇, narrow lines) and open (+, *thick lines*) conformations of the α7 model. The N-termini of the helices are at $z \approx -2$ Å; the C-termini are at $z \approx +27$ Å. (*Bottom*) The pore radius profiles for the open conformation of the α7 (◇, narrow lines) and *α7 mut* (+, *thick lines*) models are compared.

We have also performed simple continuum electrostatics calculations on these models. Although such calculations embody a number of approximations (see Discussion), they provide some valuable insights into the electrostatic environment with a model pore. In particular, they allow estimation of approximate electrostatic energy barriers and wells that a cation (M^+) experiences as it is moves along a model pore. Consider first the electrostatic energy profile for the open-state $\alpha 7$ model (Fig. 7 *A*). This reveals a potential well, of depth ~ -1.2 kcal/mol, at the C-terminal mouth of the pore. In contrast, the potential profile is rather flat at the N-terminal mouth. Analyzing the contributions made to this profile by the backbone and side-chain partial charges (see, e.g., Kerr et al., 1996) suggests that the aligned helix dipoles would generate a barrier of height ~0.5 kcal/mol at the N-terminal mouth, but that this is compensated for by the ring of E1′ side chains. A similar role for the rings of anionic side chains was suggested by Eisenman and Alvarez (1991) on the basis of calculations employing an earlier model of the nAChR pore.

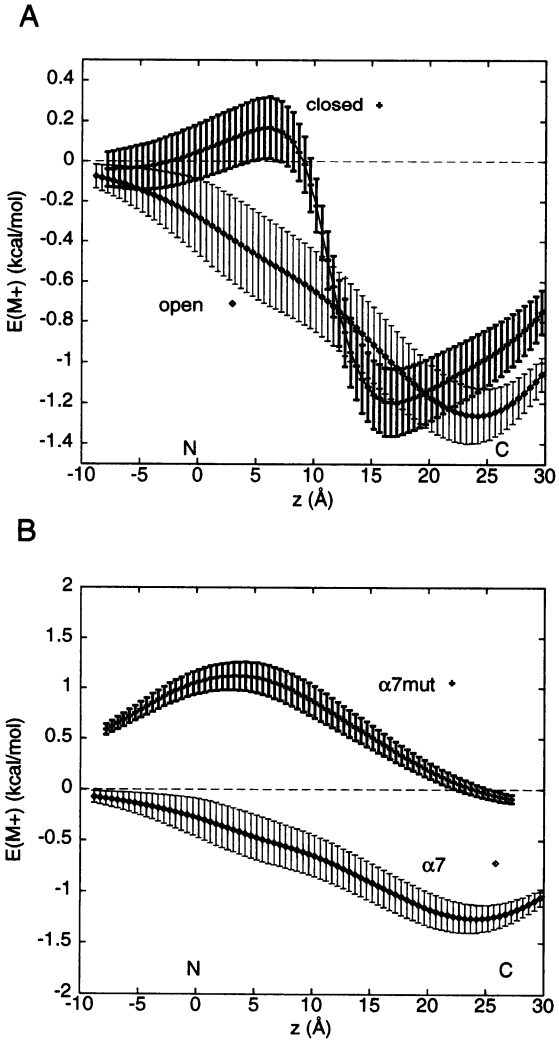

FIGURE 7 Electrostatic potential energy profiles. (*Top*) The electrostatic potential energy for an M^+ ion moved along the center of the pore (as defined by HOLE; see text for details) is compared for the open (◇, *narrow lines*) and closed (+, *thick lines*) conformations of the $\alpha 7$ model. (*Bottom*) The electrostatic potential energy profiles of $\alpha 7$ (◇) and *α7 mut* (+) model pores (both in the open conformation) are compared.

The potential profile for the $\alpha 7$ open-state pore may be compared with that of the closed-state model (Fig. 7 *A*). The two profiles are rather different. The "swiveling" of M2 about the L11′ kink results in more significant differences in the N-terminal half of the channel. The movement of the E1′ residues means that for the closed state there is a small barrier in the N-terminal half of the profile. The position of the C-terminal well is also shifted in z. The biggest difference in the profiles is the steep electrostatic potential gradient (i.e., large field) in the vicinity of the L11′ constriction of the closed pore. This is presumed to be due to the presence of the low-dielectric side chains within the lumen of the pore in the closed state. A cation entering the pore from the synaptic mouth would therefore experience two barriers to permeation: one electrostatic and one van der Waals in origin.

Comparison of the electrostatic potential profiles for the open-state model of $\alpha 7$ and of *α7 mut* (Fig. 7 *B*) is most informative. In *α7 mut*, neutralization of the negative charges at the mouths of the pore reverses the profile, such that M^+ experiences a barrier at the N-terminal mouth of the pore (because of the combined effect of the helix dipoles plus the K2′ residues). Overall a well of depth $\sim 2RT$ for M^+ passing through $\alpha 7$ is replaced by a barrier of $\sim 2RT$ for *α7 mut*. This corresponds nicely with the experimentally observed switch in ion selectivity (Galzi et al., 1992) from cationic for $\alpha 7$ to anionic for *α7 mut*. Of course, the exact height/depth of the barrier/well depends on the parameters employed in the Poisson-Boltzmann calculation (see Discussion), but the qualitative correlation remains, providing support for the modeling procedure as a whole.

Torpedo open-state models

The $\alpha 7$ nAChR is homopentameric, thus simplifying model generation by SA/MD. However, *Torpedo*, muscle, and most neuronal nAChR are heteropentameric. As the SA/MD procedure is not limited to homopentameric assemblies, it seemed reasonable to attempt to model the open state of a heteropentameric *Torpedo* nAChR pore. The sequences of the *Torpedo* M2 helices are given in Fig. 1. Note the neutralization of the N-terminal anionic residue in M2γ and of the C-terminal anionic residue in M2γ and M2δ. A priori, this is anticipated to lead to differences between the electrostatic potential profiles of heteropentameric and homopentameric models.

A possible ambiguity arises with respect to heteropentameric models of the nAChR pore in that the relative positions of the subunits within the pentamer are uncertain. Four possible subunit arrangements of the subunits are shown in Fig. 8. A model with the β subunit flanked by the two α subunits is favored by, e.g., Unwin (1995, 1996), whereas a model with γ between the two α subunits is favored by, e.g., Karlin and Akabas (1995). In the light of

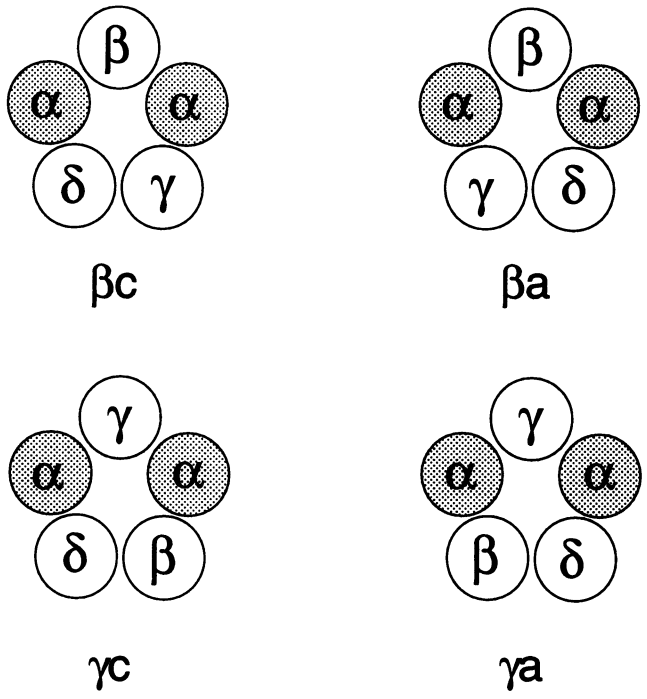

FIGURE 8 Possible configurations of the *Torpedo* pore. The view is down the pore axis from C-termini (extracellular) toward the N-termini (intracellular). Thus model βc corresponds to the β subunit between the two α subunits, with the sequence αβαγδ in clockwise order.

this ambiguity, models corresponding to all four subunit arrangements in Fig. 8 were generated. All four models were generated using the same SA/MD procedure as for the α7 open and α7 *mut* models (see above). Note that although fivefold rotational symmetry is not strictly maintained during the simulation, the target restraints are derived from a rotationally averaged EM map and so do exhibit strict rotational symmetry. Thus, significant deviations from fivefold symmetry for the polypeptide backbone of the *Torpedo* M2 bundle are absent from these models.

The pore radius profiles of the four *Torpedo* models are compared with that for α7 in Fig. 9 *A*. It can be seen that the differences between the four *Torpedo* models are insignificant. This is particularly evident if one takes into account intra-ensemble variations (not shown). However, there is a significant difference in pore radius profile from that of the α7 open state. The minimum pore radius is increased to ~6.5 Å. Furthermore, the location of the minimum pore radius is shifted toward the N-terminus. For the *Torpedo* models it corresponds to the ring of side chains formed by residue 4′. This is of interest in light of the results of Villarroel et al. (1991) and Villaroel and Sakmann (1992) that the channel conductance of *Torpedo* is particularly sensitive to changes in the size of the side chain at 4′. Models of the mutations of Villarroel et al. (1991) and Villaroel and Sakmann (1992) suggest that changes in the 4′ residue of M2α result in changes in the pore radius profile in this region (data not shown).

It is also informative to compare electrostatic potential profiles for the *Torpedo* models with that for the α7 open

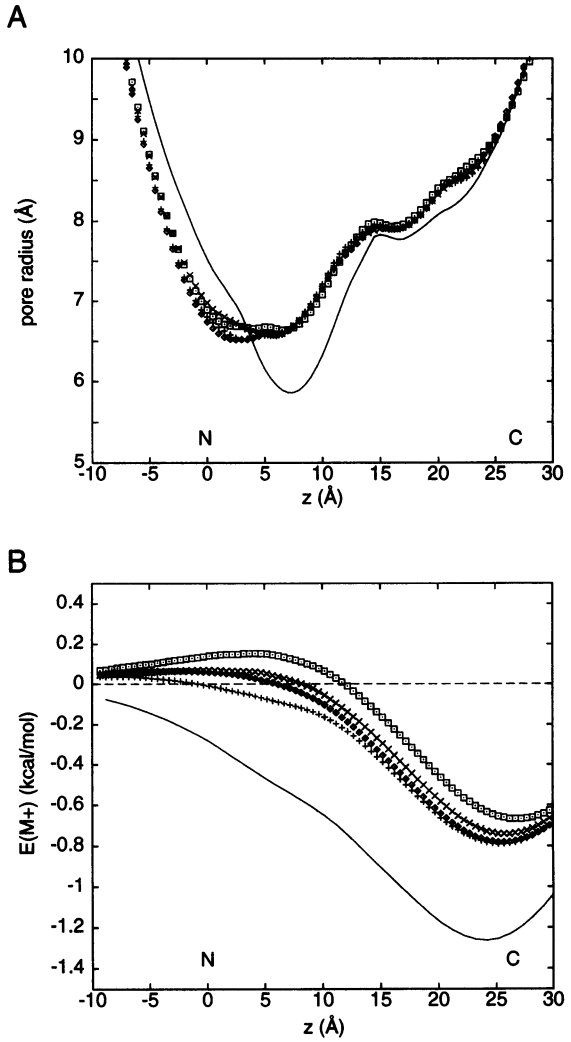

FIGURE 9 Comparison of the α7 and *Torpedo* open conformation models. (*A*) The pore radius profiles of α7 (*solid line*) and of four *Torpedo* (◇, βa; +, βc; □, γa; ×, γc) models are compared. (*B*) The electrostatic potential energy profiles for the same four *Torpedo* (◇, βa; +, βc; □, γa; ×, γc) models are given.

state (Fig. 9 *B*). Again, the differences between the different *Torpedo* profiles are small compared with the degree of intra-ensemble variation. However, there are significant differences from the α7 profile. In particular, the C-terminal potential well is shallower for the *Torpedo* models and the profile at the N-terminal mouth differs from that of α7. These small differences suggest that it may be possible to correlate the results of such approximate calculations with experimental differences between the permeation properties of the different classes of nAChR pore.

DISCUSSION

Critique of methods

The SA/MD method has been employed previously to model "simple" ion channels formed by bundles of α-heli-

ces (Kerr et al., 1994, 1996), and to model α-helix dimerization in GCN4 leucine zippers (Nilges and Brünger, 1991, 1993) and in the transmembrane domain of glycophorin (Treutlein et al., 1992). It is therefore a well-established method for identifying low-energy packing arrangements of α-helices, even though it does not necessarily yield a global minimum energy conformation, and so the resultant models will always reflect the input assumptions (see below). As a general approach to modeling, it possesses some advantages over more interactive approaches. For example, SA/MD generates an ensemble of structures for a given model. Variation within an ensemble reflects the conformational heterogeneity allowed within the confines of a given set of model restraints. Analysis of such variation provides a measure, albeit crude, of the statistical error in predictions based upon a model. There are some limitations in the SA/MD procedure, such as the absence of explicit water molecules from the lumen and the mouths of the pore. An attempt to compensate for this is made by screening of electrostatic interactions between side chains. However, the models presented in this study will require eventual refinement via MD simulations in the presence of water (Breed et al., 1996).

The second aspect of the methodology that invites appraisal is the use of EM-derived target restraints (the more technical aspects of this have been discussed in detail in an earlier paper; Sansom et al., 1995a). The main advantage of this method is that it enables inclusion of "hard" structural data within the modeling procedure. Indeed, the present study may be thought of as an attempt to integrate such structural data with less direct information from sequence and mutagenesis studies to reach a consensus model. The main limitation of the target restraints lies in the limited resolution (9 Å) of the EM data. There is also the question of the rotational symmetry that is imposed upon the structural data and hence is present in the target restraints. Because of these limitations one should avoid overinterpretation of the models.

In addition to limitations of the methodology per se, the assumptions implicit in the models require critical evaluation. The key assumption is that of the secondary structure of M2. The models presented make the simplest interpretation of the available experimental data, namely that the M2 region is α-helical. This is supported by the pattern of labeling of M2 with open-channel blockers (Hucho et al., 1986; Changeux et al., 1992), by the periodicity of M2 mutations that perturb open-channel properties (Charnet et al., 1990), by spectroscopic studies of synaptic M2 peptides (Bechinger et al., 1991; Montal, 1995), by Fourier transform infrared investigations of the nAChR transmembrane domain (Hucho et al., 1994), and by the EM data (Unwin, 1993, 1995). However, it has been suggested, on the basis of cysteine-scanning mutagenesis experiments, that the central regions of M2 may adopt a nonhelical conformation, at least in the closed state (Akabas et al., 1992, 1994; Karlin and Akabas, 1995). It may be desirable to include this possibility in future models. It should be noted that even in the current, somewhat conservative model, the central region of M2 adopts a more distorted conformation when the pore is in the closed state.

Having considered possible limitations in the modeling methodology, one must consider how correct the models are likely to be. Although the restraints on the secondary structure of the M2 segments, and on their approximate positions and orientations, may be reasonably derived from the experimental data, these restraints are not sufficient to specify a unique conformation for the backbone, let alone the side chains. A conservative estimate would suggest at least one distance restraint per residue would be required to define the overall fold of a protein backbone. Clearly, such data are not yet available for the nAChR pore domain. Furthermore, the identity of the sequence and the conformation of the polypeptide chain surrounding the M2 helix bundle remain unestablished. However, it is unlikely that the overall architecture of the M2 bundle is incorrect. In the absence of further structural data it is difficult to validate the model. One way in which this may be attempted is by using the model to predict observable physiological properties, such as ion selectivity. This is part of the rationale for the electrostatics calculations attempted in the current study. Such calculations do not allow one to establish a model as definitive, but they do provide a filter that should enable the exclusion of some incorrect models. In this fashion, modeling studies may be a envisaged as a way of reducing the number of possible models for a given channel, thus, in the longer run, enabling the design of more finely tuned experiments to probe the relationship between function and (possible) structure.

Having attempted to evaluate the modeling procedure, we have the remaining task of appraising the methods employed to analyze the resultant models. Analysis of pore geometry uses the program HOLE. This was first employed to compare the pore dimensions of different forms of the channel-forming peptide gramicidin (Smart et al., 1993) and has since been used in a number of studies of ion channels (Kerr et al., 1994, 1996; Sansom and Kerr, 1995). The principal advantage of this method is that it provides a simple and well-defined definition of the dimensions of a transbilayer pore. A possible limitation lies in the use of a column of overlapping spheres to define the radius profile of a pore. This neglects the effects of asymmetries on the pore dimensions. It is unlikely that this will be a problem with symmetrical pores, such as that of the nAChR. A modification of the method that accommodates local asymmetries is incorporated in a revision of the program (Smart et al., manuscript in preparation).

The electrostatics of the model pores have been examined using a standard Poisson-Boltzmann (PB) approach, which has been applied to a number of proteins (Harvey, 1989; Sharp and Honig, 1990; Ripoll et al., 1993; Karshikoff et al., 1994) and to lipid bilayers (Peitzsch et al., 1995). This method allows the estimation of an electrostatic potential energy profile along a pore, while attempting to take into account the screening effects of water and counterions and the inhomogeneous dielectric environment. However, it

must be realized that the method as applied in this paper is approximate. In particular, the treatment of the "solvent" within the pore probably overscreens the electrostatic potential, for two reasons. First, a dielectric of $\epsilon = 78$ is assumed for the water within the pore. Recent simulation results on the restricted dynamics of intrapore water (Chiu et al., 1991; Roux and Karplus, 1994; Engels et al., 1995; Breed et al., 1996) imply that this may be an overestimate. Preliminary simulation studies on simple α-helix bundle models (Kerr et al., 1994) of ion channels suggest that ϵ for intrapore water may be reduced by up to an order of magnitude relative to ϵ of bulk water (Sansom, manuscript in preparation). In support of this, Gutman et al. (1992) provide an experimental estimate of $\epsilon = 24$ for the water within the pore of a bacterial porin. The second approximation in the PB calculations is the assumption that the interior of the pore contains the same ionic environment (100 mM) as the bulk exterior. This appears in the PB calculation as the Debye length (κ). Thus application of the PB method to ion channel models may be improved by using suitably reduced values of ϵ and κ within the pore. Current investigations are aimed at obtaining improved estimates for these parameters. A further approximation in the PB calculations is representation of the remainder of the channel protein and the surrounding bilayer as simply a low ($\epsilon = 2$) dielectric continuum. In the absence of a model for the entire transmembrane domain of the nAChR, it is difficult to improve upon this. This should become possible as higher resolution structural data emerge. Finally, no attempt has been made to accommodate a transmembrane voltage difference in our calculations. However, despite these limitations, PB calculations do allow the electrostatic properties of channel models to be explored in a semiquantitative fashion.

Biological relevance and implications of results

The studies presented in this paper extend a sequence of models of the pore domain of the nAChR (Guy and Hucho, 1987; Furois-Corbin and Pullman, 1989a,b; Hucho and Hilgenfeld, 1989; Oiki et al., 1990; Eisenman and Alvarez, 1991; Furois-Corbin and Pullman, 1991; Ortells and Lunt, 1994, 1996; von Kitzing, 1995). All such studies have stressed the importance of the M2 helices and the channel-lining side chains. The main advance in the current models is that they incorporate the EM-derived structural data and attempt to allow for variations in side-chain conformations within the pore lining. They enable one to probe the molecular basis of channel selectivity and gating in a semiquantitative manner.

Much of this paper has focused on the α7 nAChR pore domain, modeled as a homopentamer. This involves extrapolating from structural studies on *Torpedo* nAChR to a model for a neuronal channel, but given the rotational symmetry of the target restraints, there are self-evident advantages in studying this system. Furthermore, it seems unlikely that the overall molecular architecture of the pore will differ greatly between nAChR species. It should be remembered that although α7 can form homopentameric assemblies in vitro, such homopentamers may not occur in neuronal membranes (Sivilotti and Colquhoun, 1995). However, the results of the current studies show that a similar picture of the geometry of the pore emerges whether one models α7 homopentamers or *Torpedo* heteropentamers.

Concerning the model of the α7 open state, the results of the PB calculations are in broad agreement with the experimental data. The model of an M2 pore with a ring of anionic residues at either mouth provides an electrostatic profile favorable to the permeation of cations. Future refinements to the PB assumptions may allow an improved estimate of the depth of the potential well, thus enabling comparison with experimental investigations of permeation models for the nAChR (Eisenman and Dani, 1987; Kienker et al., 1994). At first glance the dimensions of the pore in the model seem at odds with experimental estimates based on measurements of the permeability of large organic cations (Dwyer et al., 1980; Nutter and Adams, 1995). Such studies have suggested a pore radius at the narrowest point of ~3.5 Å, in contrast with a corresponding value of ~6 Å for the model. This discrepancy may simply reflect the limited resolution of the EM data. Alternatively, it may reside in the nature of the pore lining. The constriction of the pore lies in the vicinity of a ring of polar side chains: either T8′ (in α7) or T4′ and S4′ (in *Torpedo*). It is likely that in a solvated pore these residues will be associated with "bound" water molecules. For example, bound water molecules are present within the pores of the bacterial porins, as is evident from the high-resolution crystal structure of *Rhodopseudomonas blastica* porin (1PRN) (Kreusch and Schulz, 1994). In 1PRN, the minimum pore radius is 4.1 Å if one excludes the waters, whereas if the bound waters are treated as part of the pore lining, the minimum radius falls to 1.4 Å. The presence of a ring of bound waters alongside the 8′ and 4′ side-chain rings would be expected to reduce the effective minimum radius of the pore to ~3 Å, i.e., close to the experimental estimate. This aspect of the pore may emerge from the ongoing refinement of the models in the presence of explicit solvent molecules (see below). Furthermore, it is likely that passage of an ion through the channel will be correlated with the movement of side chains, which will also alter the radius of the pore as experienced by the ion.

Comparison of the open and closed models of the α7 pore provides a molecular interpretation of the "leucine ring" gating model (Labarca et al., 1995; Unwin, 1995). However, even in the closed state the pore is not completely occluded, having a minimum radius of ~2 Å. This constriction is anticipated to present an insurmountable barrier to ion permeation. Passage through such a narrow region would require the removal of most of the water of solvation from an ion. The dehydration energy of the ion would not be compensated for by a ring of hydrophobic side chains. Furthermore, it is possible that the water molecules in such a narrow region may be effectively "frozen" (Green and Lewis, 1991; Green and Lu, 1995; Sansom et al., 1996),

thus presenting a further barrier to permeation. These features may emerge in more detailed simulations of the energetics of channel/water/ion interactions. However, it should be remembered that alternatives to the "leucine ring" model of gating have been proposed (Karlin and Akabas, 1995), stressing possible involvement of the M1-M2 loop. One test of our models of the closed- and open-channel structures may be via comparison with recent mutagenesis studies of the effects of changes in the side chain at position 11′ on the open/closed equilibrium of the channel (Filatov and White, 1995; Labarca et al., 1995). These studies suggest destabilization of the closed state relative to the open when leucine at 11′ is replaced by, e.g., serine or threonine. Preliminary simulation results (Sansom, unpublished data) suggest that in the open-state model, a serine at 11′ may be able to form interhelix H-bonds within the bundle, thus providing a possible structural explanation of such mutagenesis data.

The model of the *α7 mut* pore provides an interpretation of the experimentally observed change in ion selectivity in this mutant. It appears that in this extreme case a simple electrostatic approach can explain the ion selectivity. It should be noted that our model fails to take into account the influence of the cytoplasmic ring (Imoto et al., 1988) of anionic residues, located in the M1-M2 loop. Furthermore, as emphasized by, e.g., Dorman et al. (1996), the origins of channel ion selectivity are complex, and more fine-grained theoretical tools may be required to probe more subtle aspects of selectivity.

The models presented for the *Torpedo* pore are a first approximation, as the treatment of the asymmetry of the pore (see e.g., Cohen et al., 1992; Villaroel et al., 1992) is incomplete. The shift in the narrowest region of the (open) pore from the 8′ ring to the 4′ ring in going from the α7 model to the *Torpedo* model is encouraging, as the results of, e.g., Villarroel et al. (1991) have suggested that residue 4′ forms the narrowest region of the *Torpedo* pore. The change in the electrostatic energy profile between α7 and *Torpedo* is also of interest, given the differences in permeability properties of the two classes of channel, such as the greater permeability of α7 to divalent cations.

The points of correspondence between models and experimental data for nAChR channels suggest that the overall architecture of the pore models may be correct. Clearly, it will be essential to refine such models as more structural data emerge. Indeed, an advantage of the SA/MD approach is that it facilitates such updating of the models. There are also improvements that can be made to nAChR simulations. The models are now being refined via inclusion of water within the pore during MD simulations. This will enable improved analysis of the effects of conformational flexibility of pore-lining side chains on channel properties. PB calculations may be used to analyze the likely ionization states of the rings of glutamate side chains, as has been carried out by Karshikoff et al. (1994) for *E. coli* porins. Finally, the models may be extended via inclusion of M1 segments, in an extended conformation, between the C-termini of the M2 helices (Karlin and Akabas, 1995). It is possible to extend the same modeling procedure to other members of the nAChR superfamily (Sansom and Adcock, unpublished results), to further probe the relationship between structure and function in the pore domain of ligand-gated ion channels.

Our thanks to Dr. N. Unwin (for providing us with copies of the EM results) and Dr. O. Smart (for his program HOLE). Our thanks also to other members of our group for their interest in this work, particularly to Dr. G. Smith for his critical reading of the manuscript.

This work was supported by the Wellcome Trust.

REFERENCES

Akabas, M. H., C. Kauffmann, P. Archdeacon, and A. Karlin. 1994. Identification of acetylcholine receptor channel-lining residues in the entire M2 segment of the α subunit. *Neuron.* 13:919–927.

Akabas, M. H., D. A. Stauffer, M. Xu, and A. Karlin. 1992. Acetylcholine receptor channel structure probed in cysteine-substitution mutants. *Science.* 258:307–310.

Bechinger, B., Y. Kim, L. E. Chirlian, J. Gesell, J. M. Neumann, M. Montal, J. Tomich, M. Zasloff, and S. J. Opella. 1991. Orientations of amphipathic helical peptides in membrane bilayers determined by solid-state NMR spectroscopy. *J. Biomol. NMR.* 1:167–173.

Bertrand, D., J. L. Galzi, A. Devillers-Thiéry, S. Bertrand, and J. P. Changeux. 1993. Stratification of the channel domain in neurotransmitter receptors. *Curr. Opin. Cell Biol.* 5:688–693.

Breed, J., I. D. Kerr, R. Sankararamakrishnan, and M. S. P. Sansom. 1995. Packing interactions of Aib-containing helices: molecular modelling of parallel dimers of simple hydrophobic helices and of alamethicin. *Biopolymers.* 35:639–655.

Breed, J., R. Sankararamakrishnan, I. D. Kerr, and M. S. P. Sansom. 1996. Molecular dynamics simulations of water within models of transbilayer pores. *Biophys. J.* 70:1643–1661.

Brooks, B. R., R. E. Bruccoleri, B. D. Olafson, D. J. States, S. Swaminathan, and M. Karplus. 1983. CHARMM: a program for macromolecular energy, minimisation, and dynamics calculations. *J. Comp. Chem.* 4:187–217.

Brünger, A. T. 1992. X-PLOR Version 3.1. A System for X-ray Crystallography and NMR. Yale University Press, New Haven, CT.

Changeux, J. P., J. I. Galzi, A. Devillers-Thiéry, and D. Bertrand. 1992. The functional architecture of the acetylcholine nicotinic receptor explored by affinity labelling and site-directed mutagenesis. *Q. Rev. Biophys.* 25:395–432.

Charnet, P., C. Labarca, R. J. Leonard, N. J. Vogelaar, L. Czyzyk, A. Gouin, N. Davidson, and H. A. Lester. 1990. An open-channel blocker interacts with adjacent turns of α-helices in the nicotinic acetylcholine receptor. *Neuron.* 2:87–95 .

Chiu, S. W., E. Jakobsson, S. Subramanian, and J. A. McCammon. 1991. Time-correlation analysis of simulated water motion in flexible and rigid gramicidin channels. *Biophys. J.* 60:273–285.

Cohen, B. N., C. Labarca, L. Czyzk, N. Davidson, and H. Lester. 1992. $Tris^+/Na^+$ permeability ratios of nicotinic acetylcholine receptors are reduced by mutations near the intracellular end of the M2 region. *J. Gen. Physiol.* 99:545–572.

Couturier, S., D. Bertrand, J.-M. Matter, M.-C. Hernandez, S. Bertrand, N. Millar, S. Valera, T. Barkas, and M. Ballivet. 1990. A neuronal nicotinic acetylcholine receptor subunit (alpha 7) is developmentally regulated and forms a homooligomeric channel blocked by alpha BTX. *Neuron.* 5:847–856.

Davis, M. E., J. D. Madura, B. A. Luty, and J. A. McCammon. 1991. Electrostatics and diffusion of molecules in solution: simulations with the University of Houston Brownian dynamics program. *Comput. Phys. Comm.* 62:187–197.

Dorman, V., M. B. Partenskii, and P. C. Jordan. 1996. A semi-microscopic Monte Carlo study of permeation energetics in a gramicidin-like channel: the origin of cation selectivity. *Biophys. J.* 70:121–134.

Dwyer, T. M., D. J. Adams, and B. Hille. 1980. The permeability of the endplate channel to organic cations in frog muscle. *J. Gen. Physiol.* 75:469–492.

Eisenman, G., and O. Alvarez. 1991. Structure and function of channels and channelogs as studied by computational chemistry. *J. Membr. Biol.* 119:109–132.

Eisenman, G., and J. A. Dani. 1987. An introduction to molecular architecture and permeability of ion channels. *Annu. Rev. Biophys. Biophys. Chem.* 16:205–226.

Engels, M., D. Bashford, and M. R. Ghadiri. 1995. Structure and dynamics of self-assembling peptide nanotubes and the channel-mediated water organization and self-diffusion. A molecular dynamics study. *J. Am. Chem. Soc.* 117:9151–9158.

Filatov, G. N., and M. M. White. 1995. The role of conserved leucines in the M2 domain of the acetylcholine-receptor in channel gating. *Mol. Pharmacol.* 48:379–384.

Furois-Corbin, S., and A. Pullman. 1989a. Energy profiles in the acetylcholine receptor (AChR) channel. *FEBS Lett.* 252:63–68.

Furois-Corbin, S., and A. Pullman. 1989b. A possible model for the inner wall of the acetylcholine receptor channel. *Biochim. Biophys. Acta.* 984:339–350.

Furois-Corbin, S., and A. Pullman. 1991. The effect of point mutations on energy profiles in a model of the nicotinic acetylcholine (AChR) channel. *Biophys. Chem.* 39:153–159.

Galzi, J. L., and J. P. Changeux. 1994. Neurotransmitter-gated ion channels as unconventional allosteric proteins. *Curr. Opin. Struct. Biol.* 4:554–565.

Galzi, J. L., A. Devillers-Thiery, N. Hussy, S. Bertrand, J. P. Changeux, and D. Bertrand. 1992. Mutations in the channel domain of a neuronal nicotinic receptor convert ion selectivity from cationic to anionic. *Nature.* 359:500–505.

Gilson, M. K., K. A. Sharp, and B. H. Honig. 1988. Calculating the electrostatic potential of molecules in solution: method and error assessment. *J. Comp. Chem.* 9:327–335.

Giraudat, J., M. Dennis, T. Heidmann, P. Y. Haumont, F. Lederer, and J. P. Changeux. 1987. Structure of the high-affinity binding site for noncompetitive blockers of the acetylcholine receptor: [^{3}H]chlorpromazine labels homologous residues in the α and δ chains. *Biochemistry.* 26: 2410–2418.

Green, M. E., and J. Lewis. 1991. Monte Carlo simulation of the water in a channel with charges. *Biophys. J.* 59:419–426.

Green, M. E., and J. Lu. 1995. Monte-Carlo simulations of the effects of charges on water and ions in a tapered pore. *J. Colloid Interface Sci.* 171:117–126.

Gutman, M., Y. Tsfadia, A. Masad, and E. Nachiel. 1992. Quantitation of physical-chemical properties of the aqueous phase inside the phoE ionic channel. *Biochim. Biophys. Acta.* 1109:141–148.

Guy, H. R., and F. Hucho. 1987. The ion channel of the nicotinic acetylcholine receptor. *Trends Neurosci.* 10:318–321.

Harvey, S. C. 1989. Treatment of electrostatic effects in macromolecular modelling. *Proteins Struct. Funct. Genet.* 5:78–92.

Hucho, F., U. Görne-Tschelnokow, and A. Strecker. 1994. β-Structure in the membrane-spanning part of the nicotinic acetylcholine receptor (or how helical are transmembrane helices?). *Trends Biochem. Sci.* 19: 383–387.

Hucho, F., and R. Hilgenfeld. 1989. The selectivity filter of a ligand-gated ion channel. *FEBS Lett.* 257:17–23.

Hucho, F., W. Oberthür, and F. Lottspeich. 1986. The ion channel of the nicotinic acetylcholine receptor is formed by the homologous helices M II of the receptor subunits. *FEBS Lett.* 205:137–142.

Imoto, K., C. Busch, B. Sakmann, M. Mishina, T. Konno, J. Nakai, H. Buyo, Y. Mori, K. Kukuda, and S. Numa. 1988. Rings of negatively charged amino acids determine the acetylcholine receptor channel conductance. *Nature.* 335:645–648.

Karlin, A., and M. H. Akabas. 1995. Toward a structural basis for the function of nicotinic acetylcholine receptors and their cousins. *Neuron.* 15:1231–1244.

Karshikoff, A., V. Spassov, S. W. Cowan, R. Ladenstein, and T. Schirmer. 1994. Electrostatic properties of two porin channels from *Escherichia coli*. *J. Mol. Biol.* 240:372–384.

Kerr, I. D., D. G. Doak, R. Sankararamakrishnan, J. Breed, and M. S. P. Sansom. 1996. Molecular modelling of staphylococcal δ-toxin ion channels by restrained molecular dynamics. *Protein Eng.* 9:161–171.

Kerr, I. D., R. Sankararamakrishnan, O. S. Smart, and M. S. P. Sansom. 1994. Parallel helix bundles and ion channels: molecular modelling via simulated annealing and restrained molecular dynamics. *Biophys. J.* 67:1501–1515.

Kerr, I. D., and M. S. P. Sansom. 1993. Hydrophilic surface maps of α-helical channel-forming peptides. *Eur. Biophys. J.* 22:269–277.

Kienker, P., G. Tomaselli, M. Jurman, and G. Yellen. 1994. Conductance mutations of the nicotinic acetylcholine receptor do not act by a simple electrostatic mechanism. *Biophys. J.* 66:325–334.

Kraulis, P. J. 1991. MOLSCRIPT: a program to produce both detailed and schematic plots of protein structures. *J. Appl. Cryst.* 24:946–950.

Kreusch, A., and G. E. Schulz. 1994. Refined structure of the porin from *Rhodobacter blastica*. *J. Mol. Biol.* 243:891–905.

Labarca, C., M. W. Nowak, L. Tang, P. Deshpande, N. Davidson, and H. Lester. 1995. Leucine residues at the 9 position of the M2 domain in AChR govern EC50 independently and symmetrically. *Biophys. J.* 68: A233.

Leonard, R. J., C. G. Labarca, P. Charnet, N. Davidson, and H. A. Lester. 1988. Evidence that the M2 membrane-spanning region lines the ion channel pore of the nicotinic receptor. *Science.* 242:1578–1581.

Lester, H. 1992. The permeation pathway of neurotransmitter-gated ion channels. *Annu. Rev. Biophys. Biomol. Struct.* 21:267–292.

Montal, M. 1995. Design of molecular function: channels of communication. *Annu. Rev. Biophys. Biomol. Struct.* 24:31–57.

Moore, W. J. 1972. Physical Chemistry. Longman, London.

Nicholls, A., and B. Honig. 1992. GRASP Manual. Columbia University, New York.

Nilges, M., and A. T. Brünger. 1991. Automated modelling of coiled coils: application to the GCN4 dimerization region. *Protein Eng.* 4:649–659.

Nilges, M., and A. T. Brünger. 1993. Successful prediction of the coiled coil geometry of the GCN4 leucine zipper domain by simulated annealing: comparison to the X ray structure. *Proteins Struct. Funct. Genet.* 15:133–146.

Nutter, T. J., and D. J. Adams. 1995. Monovalent and divalent cation permeability and block of neuronal nicotinic receptor channels in rat parasympathetic ganglia. *J. Gen. Physiol.* 105:701–723.

Oiki, S., W. Danho, V. Madison, and M. Montal. 1988. M2δ, a candidate for the structure lining the ionic channel of the nicotinic cholinergic receptor. *Proc. Natl. Acad. Sci. USA.* 85:8703–8707.

Oiki, S., V. Madison, and M. Montal. 1990. Bundles of amphipathic transmembrane α-helices as a structural motif for ion conducting channel proteins: studies on sodium channels and acetylcholine receptors. *Proteins Struct. Funct. Genet.* 8:226–236.

Ortells, M. O., and G. G. Lunt. 1994. The transmembrane region of the nicotinic acetylcholine receptor: is it an all-helix bundle? *Receptors Channels.* 2:53–59.

Ortells, M. O., and G. G. Lunt. 1996. A mixed helix-beta-sheet model of the transmembrane region of the nicotinic acetylcholine receptor. *Protein Eng.* 9:51–59.

Peitzsch, R. M., M. Eisenberg, K. A. Sharp, and S. McLaughlin. 1995. Calculations of the electrostatic potential adjacent to model phospholipid bilayers. *Biophys. J.* 68:729–738.

Ripoll, D. R., C. H. Faerman, P. H. Axelsen, I. Silman, and J. L. Sussman. 1993. An electrostatic mechanism for substrate guidance down the aromatic gorge of acetylcholineesterase. *Proc. Natl. Acad. Sci. USA.* 90:5128–5132.

Roux, B., and M. Karplus. 1994. Molecular dynamics simulations of the gramicidin channel. *Annu. Rev. Biophys. Biomol. Struct.* 23:731–761.

Sankararamakrishnan, R., and M. S. P. Sansom. 1995a. Modelling packing interactions in parallel helix bundles: pentameric bundles of nicotinic receptor M2 helices. *Biochim. Biophys. Acta.* 1239:122–132.

Sankararamakrishnan, R., and M. S. P. Sansom. 1995b. Structural features of isolated M2 helices of nicotinic receptors. Simulated annealing via molecular dynamics studies. *Biophys. Chem.* 55:215–230.

Sansom, M. S. P. 1995. Twist to open. *Curr. Biol.* 5:373–375.

Sansom, M. S. P., and I. D. Kerr. 1995. Transbilayer pores formed by β-barrels: molecular modelling of pore structures and properties. *Biophys. J.* 69:1334–1343.

Sansom, M. S. P., I. D. Kerr, J. Breed, and R. Sankararamakrishnan. 1996. Water in channel-like cavities: structure and dynamics. *Biophys. J.* 70:693–702.

Sansom, M. S. P., R. Sankararamakrishnan, and I. D. Kerr. 1995a. Modelling membrane proteins using structural restraints. *Nature Struct. Biol.* 2:624–631.

Sansom, M. S. P., H. S. Son, R. Sankararamakrishnan, I. D. Kerr, and J. Breed. 1995b. Seven-helix bundles: molecular modelling via restrained molecular dynamics. *Biophys. J.* 68:1295–1310.

Sharp, K. A., and B. Honig. 1990. Electrostatic interactions in macromolecules: theory and applications. *Annu. Rev. Biophys. Biophys. Chem.* 19:301–332.

Sivilotti, L., and D. Colquhoun. 1995. Acetylcholine receptors: too many channels, too few functions. *Science.* 269:1681–1682.

Smart, O. S., J. M. Goodfellow, and B. A. Wallace. 1993. The pore dimensions of gramicidin A. *Biophys. J.* 65:2455–2460.

Stroud, R. M., M. P. McCarthy, and M. Shuster. 1990. Nicotinic acetylcholine receptor superfamily of ligand gated ion channels. *Biochemistry.* 29:11009–11023.

Treutlein, H. R., M. A. Lemmon, D. M. Engelman, and A. T. Brunger. 1992. The glycophorin A transmembrane domain dimer: sequence specific propensity for a right handed supercoil of helices. *Biochemistry.* 31:12726–12733.

Unwin, N. 1993. Nicotinic acetylcholine receptor at 9 Å resolution. *J. Mol. Biol.* 229:1101–1124.

Unwin, N. 1995. Acetylcholine receptor channel imaged in the open state. *Nature.* 373:37–43.

Unwin, N. 1996. Projection structure of the nicotinic acetylcholine receptor: distinct conformations of the α subunits. *J. Mol. Biol.* 257: 586–596.

Villarroel, A., S. Herlitze, M. Koenen, and B. Sakmann. 1991. Location of a threonine residue in the a-subunit M2 transmembrane segment that determines the ion flow through the acetylcholine receptor channel. *Proc. R. Soc. Lond. B.* 243:69–74.

Villaroel, A., S. Herlitze, V. Witzemann, M. Koenen, and B. Sakmann. 1992. Asymmetry of the rat acetylcholine receptor subunits in the narrow region of the pore. *Proc. R. Soc. Lond. B.* 249:317–324.

Villaroel, A., and B. Sakmann. 1992. Threonine in the selectivity filter of the acetylcholine receptor channel. *Biophys. J.* 62:196–205.

von Kitzing, E. 1995. Structure modeling of the acetylcholine receptor channel and related ligand gated channels. *In* Modelling of Biomolecular Structures and Mechanisms. A. Pullman, editor. Dordrecht, Kluwer. 39–57.